Vol. 67: 77–89, 2012
doi: 10.3354/ame01584

AQUATIC MICROBIAL ECOLOGY
Aquat Microb Ecol

Published online September 11

Autotrophic and heterotrophic microbial plankton biomass in the NW Iberian upwelling: seasonal assessment of metabolic balance

O. Espinoza-González[1], F. G. Figueiras[1,*], B. G. Crespo[1,2], I. G. Teixeira[1], C. G. Castro[1]

[1]**Instituto de Investigacións Mariñas, CSIC, Eduardo Cabello 6, 36208 Vigo, Spain**

[2]***Present address:*** **Departament de Biología i Oceanografía, Institut de Ciències del Mar, CSIC, 08003 Barcelona, Spain**

ABSTRACT: Although it is assumed that small plankton cells prevail in the oligotrophic ocean and microplankton dominate in coastal upwelling zones, several signals point to a great importance of pico- and nanoplankton in upwelling systems. We studied the size distribution of autotrophic and heterotrophic microbial plankton biomass in shelf waters of the NW Iberian upwelling over an annual cycle. Both autotrophs and heterotrophs showed a seasonal evolution related to the hydrographic regime. The lowest total plankton biomass (3.8 ± 0.9 g C m^{-2}) was recorded in winter associated with the Iberian Poleward Current, while highest values occurred during the spring onset (10.5 ± 3.4 g C m^{-2}), summer upwelling (10.8 ± 3.8 g C m^{-2}) and summer stratification (9.3 ± 2.0 g C m^{-2}). Nano- and picoplankton dominated the microbial community, with the major variations in biomass occurring through the addition or disappearance of microplankton cells, mainly diatoms. Thus, the food web in this upwelling system should be considered multivorous, with the microbial loop (pico- and nanoplankton) as a background to which a diatom-based food web is added during upwelling. The estimated metabolic balance showed that the microbial community was autotrophic only during upwelling and spring onset, coinciding with the presence of diatoms. Heterotrophy was basically located in the picoplankton fraction. These results and the threshold of carbon fixation (2.5 to 3.5 g C m^{-2} d^{-1}) needed to maintain a balanced metabolism lead us to conclude that in a future scenario with low upwelling intensity and frequency, the microbial community in the NW Iberian upwelling would be heterotrophic.

KEY WORDS: Microbial plankton · Size structure · Picoplankton · Nanoplankton · Diatoms · Upwelling-downwelling · Multivorous food web · NW Iberia

INTRODUCTION

Coastal upwelling systems, due to nutrient enrichment of the surface layer with newly upwelled water, have traditionally been considered areas of the world's oceans in which the microbial community is dominated by large phytoplankton (Ryther 1969, Margalef 1978). Because of this, it is commonly assumed that the herbivorous food web prevails in these highly productive regions (Cushing 1989), where export of photosynthesised organic matter outside the microbial realm is considerable (Goldman 1988, Cushing 1989). Nevertheless, upwelling is not an exclusive oceanographic process taking place in these coastal zones since downwelling is equally important. The effect of downwelling is, however, completely opposite to that induced by upwelling. Thus, downwelling and even upwelling relaxation causes the coastward advection of warm and nutrient-poor surface oceanic waters (Crespo et al. 2007), in which

*Corresponding author. Email: paco@iim.csic.es

small-sized plankton cells (Ryther 1969) and therefore the microbial food web predominate (Pomeroy 1974, Azam et al. 1983).

Pico- and nanoplankton dominance during downwelling or upwelling relaxation has been well documented in several coastal upwelling systems (e.g. Varela et al. 1991, Tilstone et al. 2003, Iriarte & González 2004, Lorenzo et al. 2005, Sherr et al. 2005, Böttjer & Morales 2007). However, it is still relatively unknown whether the dominance of these small plankton cells is established through substitution of microplankton or, in contrast, occurs because microplankton vanish during non-upwelling conditions. Identifying which of these 2 processes (addition-disappearance vs. substitution of microplankton) takes place is relevant because it affects the structure and function of the pelagic food web and, hence, the fate of carbon fixed by autotrophs in coastal upwelling systems (Cushing 1989). Substitution between microplankton and small plankton cells means that a herbivorous food web based on diatoms alternates with the microbial loop based on small phytoplankton (Ryther 1969, Cushing 1989, Barber & Hiscock 2006). In contrast, addition-disappearance of microplankton to-from a microbial community composed of smaller cells implies that the microbial loop is a permanent feature in coastal upwelling systems (Teixeira et al. 2011) and that a multivorous food web (Legendre & Rassoulzadegan 1995) better characterises these ecosystems (Vargas et al. 2007, Linacre et al. 2010, Teixeira et al. 2011).

To elucidate how the microbial food web in coastal upwelling systems is organised, we explored the seasonal and short-term (1 wk) variability of the structure and composition of the microbial plankton community at the continental shelf in the NW Iberian margin (Fig. 1). The wind regime in this coastal upwelling region shows a clear seasonal signal (Wooster et al. 1976, Figueiras et al. 2002), with upwelling-favourable equatorward winds blowing from April to the end of September and downwelling-favourable poleward winds lasting from October to March. However, seasonality only accounts for a small part (<30%) of the total annual variability in the wind regime, with most of the variability occurring at shorter time scales (Álvarez-Salgado et al. 2003). This indicates that relaxation and even opposite events within a given upwelling or downwelling season are frequent (Figueiras et al. 2002). Although interannual variability in the onset and cessation of each season also occurs (Figueiras et al. 2002, Álvarez-Salgado et al. 2003), seasonal upwelling-downwelling transition usually coincides or precedes

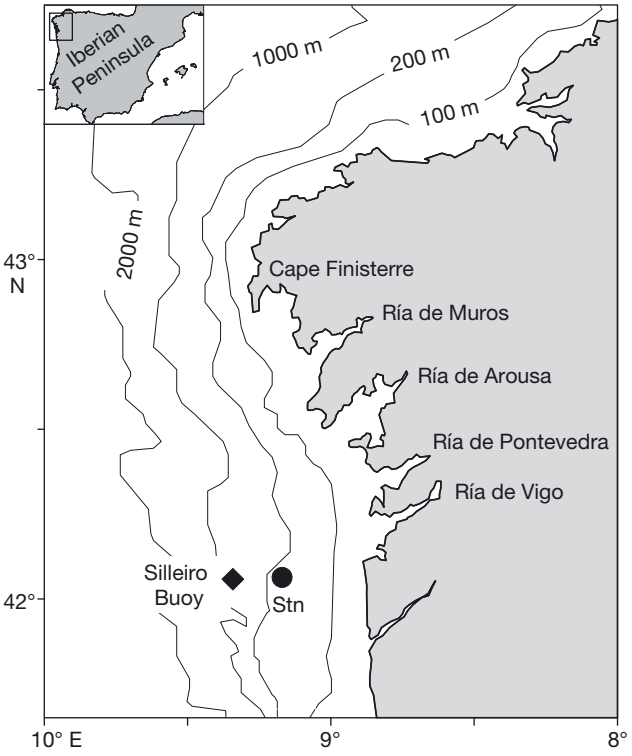

Fig. 1. The NW Iberian margin showing the location of the sampled station (●) and the position of the Silleiro buoy (◆) where the winds used to estimate cross-shore Ekman transport were recorded. The location of the 4 Rías Baixas is also shown

the onset of the Iberian Poleward Current (IPC) (Álvarez-Salgado et al. 2003, Torres & Barton 2006). The IPC is a northward surface flow on the slope that originates at southernmost latitudes (Frouin et al. 1990, Peliz et al. 2005, Crespo & Figueiras 2007) from the advection of warm and saline oceanic water to the continental shelf. Summer upwelling and the IPC are among the oceanographic features with the highest influence on plankton distributions in the NW Iberian region (e.g. Fermín et al. 1996, Castro et al. 1997, Crespo et al. 2007).

MATERIALS AND METHODS

Sampling

A station located on the shelf (150 m depth) in front of the Ría de Vigo (42° 07.8′ N, 9° 10.2′ W) was visited weekly on board the RV 'Mytilus' from 15 May 2001 to 24 April 2002 (Fig. 1). Sampling took place by means of a rosette equipped with PVC Niskin bottles to which a conductivity, temperature and depth sensor (CTD) fitted with a fluorometer and a spherical

light sensor (Biospherical) was attached. Seawater samples to determine nitrate and chlorophyll *a* (chl *a*) concentrations as well as autotrophic and heterotrophic microbial plankton biomass were collected from the CTD upcasts. A LI-190SA cosine-sensor placed on deck recorded the incident irradiance at the sea surface at 1 min intervals.

Wind and Ekman transport

Wind direction and velocity, recorded every hour at the Silleiro buoy (Fig. 1) deployed by the Spanish Agency Puertos del Estado, were used to estimate Ekman transport (Q_x; $m^2\ s^{-1}$) perpendicular to the coast according to Bakun (1973):

$$Q_x = \frac{\rho_a C |V| V_y}{f \rho_w} \quad (1)$$

where ρ_a is the air density (1.22 kg m^{-3}), C is an empirical drag coefficient (1.3×10^{-3}, dimensionless), $|V|$ is the wind speed (m s^{-1}) with component V_y, f is the Coriolis parameter at this latitude ($9.95 \times 10^{-5}\ s^{-1}$), and ρ_w is the density of seawater (~1025 kg m^{-3}). The sign of Q_x was changed to associate positive values with offshore transport (upwelling) of surface waters.

Nitrate and chl *a*

Nitrate and chl *a* levels were determined at 7 to 8 depths in the water column from surface to bottom. Nitrate concentrations (µmol kg^{-1}) were determined by segmented flow analysis with Alpkem autoanalysers (Hansen & Grasshoff 1983). For chl *a* determinations, seawater volumes of 100 to 250 ml were filtered through 25 mm Whatman glass fiber filters (GF/F) under low vacuum pressure. The filters were immediately frozen at −20°C until pigments were extracted in 90% acetone over 24 h in the dark at 4°C. Chl *a* concentration (mg m^{-3}) was determined by fluorescence of the pigment extracts using a Turner Designs fluorometer calibrated with pure chl *a* (Sigma Chemical).

Microbial plankton biomass

Samples to determine autotrophic and heterotrophic microbial plankton biomass were collected from 4 to 5 depths within the photic layer, which varied between 27 and 88 m (Fig. 2e, Table 1). Sampling depths were selected after inspecting the

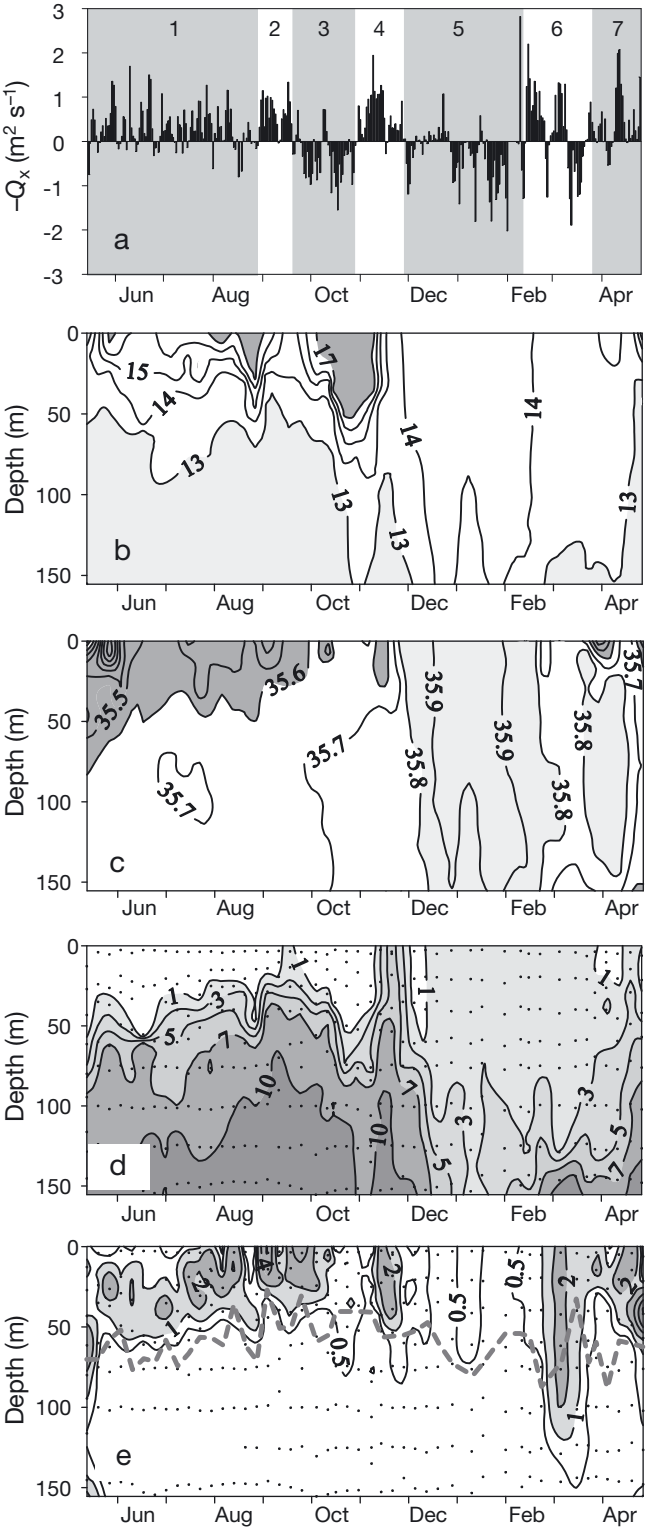

Fig. 2. Evolution of (a) cross-shore Ekman transport, (b) temperature (°C), (c) salinity, (d) nitrate concentration (µmol kg^{-1}), and (e) chlorophyll *a* concentration (mg m^{-3}) at the sampled station. The dashed line in (e) shows the depth of the photic layer (0.1% of surface irradiance). The 7 hydrographic phases (1 to 7) are given in Panel (a)

Table 1. Average (±1 SD) total microbial plankton biomass (TC), autotrophic plankton biomass (AC), heterotrophic plankton biomass (HC) and chlorophyll *a* (chl *a*) concentration (mg m^{-2}) integrated over the photic layer ($Z_{0.1\%}$) for the 7 hydrographic phases identified and the whole sampling period. $Z_{0.1\%}$ is the average (±SD) depth (m) of the photic layer (0.1% of surface irradiance); n = number of samples; IPC: Iberian Poleward Current

Hydrographic phase	Biomass (g C m^{-2})			Chl *a*	$Z_{0.1\%}$
	TC	AC	HC		
Phase 1 (n = 16) Summer stratification	9.3 ± 2.0	3.7 ± 1.1	5.6 ± 1.6	78 ± 24	63 ± 10
Phase 2 (n = 4) Summer upwelling	10.8 ± 3.8	6.1 ± 3.6	4.7 ± 0.7	97 ± 28	40 ± 12
Phase 3 (n = 5) Autumn downwelling	5.6 ± 2.1	2.6 ± 1.2	3.0 ± 1.0	45 ± 18	47 ± 9
Phase 4 (n = 4) Winter upwelling	5.2 ± 1.1	2.5 ± 0.9	2.7 ± 0.4	71 ± 54	51 ± 7
Phase 5 (n = 8) IPC	3.8 ± 0.9	1.6 ± 0.4	2.2 ± 0.5	30 ± 9	61 ± 11
Phase 6 (n = 5) Winter mixing	5.8 ± 2.5	3.4 ± 1.8	2.4 ± 0.8	76 ± 54	64 ± 21
Phase 7 (n = 5) Spring onset	10.5 ± 3.4	5.7 ± 2.0	4.8 ± 1.5	107 ± 54	66 ± 12
Whole sampling period (n = 47)	7.5 ± 3.3	3.5 ± 2.0	4.0 ± 1.8	70 ± 39	59 ± 14

fluorescence profiles to ensure that the subsurface chlorophyll maximum (SCM) was sampled when it was present. Subsamples of 10 ml were fixed with buffered 0.2 µm filtered formaldehyde (2% final concentration) and stained with DAPI at 0.1 µg ml^{-1} final concentration for 10 min in the dark (Porter & Feig 1980). The samples were then filtered through 0.2 µm black Millipore-Isopore filters placed on top of 0.45 µm Millipore backing filters. Epifluorescence microscopy was used to identify autotrophic and heterotrophic pico- and nanoplankon. Autotrophic organisms were enumerated under blue light excitation, and heterotrophic organisms were counted under excitation with UV light. It was assumed that all organisms showing red autofluorescence when excited with blue light were autotrophic, even though mixotrophic organisms are not correctly identified with this technique. However, *Prochlorococcus*, which is also inadequately identified and counted with this technique, has a limited presence in the region. Its occurrence in shelf waters of NW Iberia is restricted to short time periods in autumn, coinciding with the seasonal upwelling-downwelling transition when oceanic waters are advected over the shelf (Rodríguez et al. 2006). The biomass of heterotrophic bacteria was estimated using a conversion factor (17.4 fg C $cell^{-1}$) previously determined for the study region (Morán et al. 2002). Dimensions were taken for several individuals of the other plankton groups, and cell volumes were calculated assuming a spherical shape or after approximation to the nearest geometrical shape (Hillebrand et al. 1999). Cell carbon was estimated following Bratbak & Dundas (1984) for *Synechococcus*-type cyanobacteria, Verity et al. (1992) for pico- and nanoflagellates and Strathmann (1967) for small naked dinoflagellates recorded in the nano-size fraction.

For microplankton determination, samples (100 ml) preserved in Lugol's iodine were sedimented in composite sedimentation chambers and observed with an inverted microscope. The organisms were counted and identified to the species level when possible. The small species were enumerated from 2 transects scanned at 400× and 250×, whereas the larger species were counted from scanning the whole slide at 100×. Phototrophic and heterotrophic species of dinoflagellates, flagellates and ciliates were differentiated following Lessard & Swift (1986) and also using our historical records of epifluorescence microscopy. Cell biovolumes were estimated according to Hillebrand et al. (1999), and cell carbon was calculated following Strathmann (1967) for diatoms and dinoflagellates, Verity et al. (1992) for flagellates, Verity & Langdon (1984) for loricate ciliates and Putt & Stoecker (1989) for aloricate ciliates. All organisms containing chloroplasts were assumed to be autotrophic. Ciliates <20 µm and single diatoms <20 µm counted with this technique were assigned to the nanoplankton fraction. In contrast, chain-forming diatoms with cells <20 µm were assumed to be microplankton.

As vertical distributions of all plankton groups are rather similar and roughly follow chl *a* distribution (Fig. 2e), results of microbial plankton biomass are shown integrated over the photic zone. Integration was done at 1 m intervals from the sea surface down to 0.1% of the surface irradiance.

RESULTS

Meteorology and hydrography

Wind forcing and the hydrographic response of the water column have been previously described in

detail by Crespo et al. (2007). Briefly, 7 phases recorded in wind forcing induced discernible responses in the water column (Fig. 2). Extremely variable northerly winds during Phase 1 (Fig. 2a) were unable to cause upwelling on the shelf. Although the water column during this phase remained stratified (Fig. 2b,c) with low nitrate concentrations (<1 µmol kg^{-1}) in the surface layer (Fig. 2d), upwelling-favourable northerly winds forced the continuous uplift of the nitracline (Fig. 2d) and its SCM (Fig. 2e). Phase 1 ended with a period of wind relaxation during the second half of August (Fig. 2a) that caused a short downwelling event. This downwelling is easily discernible from the downward orientation of the temperature and nitrate isolines (Fig. 2b,d) and the decrease in chl *a* concentrations to values <1 mg m^{-3} (Fig. 2e) recorded at the end of this Phase 1.

Upwelling and downwelling alternated during the next 3 phases. Persistent northerly winds defined Phase 2 (Fig. 2a), which lasted from 30 August to 24 September. The nutrients supplied to the surface layer during this upwelling event (Fig. 2d) fuelled a conspicuous increase in chl *a* concentrations (Fig. 2e). After this upwelling, there was a month (25 September to 30 October) with dominance of southerly winds (Phase 3; Fig. 2a) that caused downwelling. This downwelling, which was longer and stronger than the preceding one at the end of Phase 1, also caused a reduction in chl *a* concentrations to values <1 mg m^{-3} (Fig. 2e). A new intense upwelling that injected nutrients into the surface layer (Fig. 2d) favouring an increase in chl *a* concentration (Fig. 2e) occurred during the next period, Phase 4, in November (Fig. 2a).

Winter conditions started with Phase 5, when variable southerly winds (Fig. 2a) coincided with the presence of the IPC in the region. The IPC was characterised by a homogeneous water body of 14°C (Fig. 2b) and salinity >35.8 (Fig. 2c), with relatively low nitrate (<3 µmol kg^{-1}) and chl *a* (~0.5 mg m^{-3}) concentrations. Winds during Phase 6 changed from upwelling- to downwelling-favourable (Fig. 2a). In this phase, with high water column homogenisation (Fig. 2b,c), chl *a* concentration began to increase, showing a uniform vertical distribution (Fig. 2e). The spring transition from winter homogenisation to summer stratification took place during the last period, Phase 7. In this period, upwelling (Fig. 2a) coincided with the early development of temperature stratification in the surface layer (Fig. 2b) and a noticeable increase in chl *a* concentration (Fig. 2e).

Seasonal variability in microbial plankton biomass: trophic and size structure

Both integrated autotrophic (AC) and heterotrophic plankton carbon (HC) biomasses, and consequently total microbial plankton carbon biomass (TC), showed a clear seasonal evolution (Fig. 3a, Table 1), with the lowest values of TC during the IPC (Phase 5) and the highest during the summer upwelling (Phase 2). High values of TC were also recorded during summer stratification (Phase 1) and at the spring onset (Phase 7). Despite the similar seasonal variability in AC and HC (Fig. 3a), changes between hydrographic phases were more frequent and pronounced in AC than in HC (Table 1). Thus, a significant change ($p < 0.05$, *t*-test for 2 samples) occurred between summer stratification (Phase 1) and summer upwelling (Phase 2), when AC almost doubled. After that, AC decreased to less than half of its maximum during the autumn downwelling (Phase 3). Another significant reduction in AC took place between the winter upwelling (Phase 4) and the IPC (Phase 5). Following this reduction, AC increased to reach values at the spring onset (Phase 7) similar to those recorded during the summer upwelling (Phase 2). In contrast, HC only experienced 2 significant changes ($p < 0.05$, *t*-test for 2 samples). The first was the reduc-

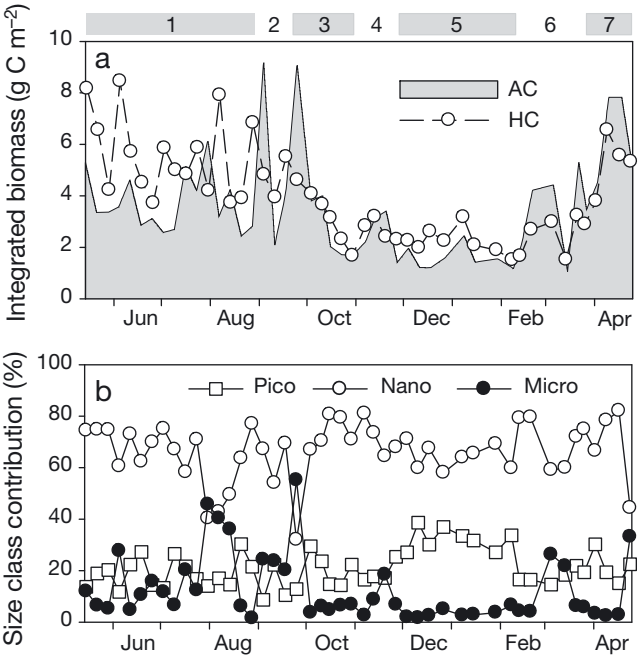

Fig. 3. Evolution of (a) integrated biomass over the photic layer of autotrophic (AC) and heterotrophic (HC) plankton and (b) contribution of (Pico) picoplankton, (Nano) nanoplankton and (Micro) microplankton to total microbial plankton biomass. The 7 hydrographic phases (1 to 7) are given above Panel (a)

tion that took place between Phases 2 and 3; the second one was the increase observed between Phases 6 and 7. HC remained relatively constant at ~2.5 g C m^{-2} during the phases in between (Table 1).

Changes were also observed in the size structure of the microbial community (Fig. 3b), which was largely dominated by nanoplankton (66 ± 11% [SD here and elsewhere] of TC). The microplankton fraction, representing 12 ± 13% of TC over the whole sampling period, gained importance at the end of the stratification period (Phase 1) and during the upwelling of Phase 2, when this fraction accounted for 31 ± 14% of TC. The contribution of microplankton was especially important at the end of this upwelling phase (55% of TC). Although of less importance, microplankton contributions exceeding the seasonal average value were registered on some occasions during Phases 4 (18%), 6 (24 ± 3%) and 7 (33%). In contrast, microplankton biomass (0.13 ± 0.6 g C m^{-2}) and their contribution to TC (4 ± 2%) were extremely low during the IPC (Phase 5). During this phase (Fig. 3b), picoplankton achieved greater importance (32 ± 5% of TC), well above their mean seasonal contribution (21 ± 7%). The size structure of the microbial community in the SCM of the stratified Phase 1 (Fig. 2e) did not differ ($p > 0.26$, *t*-test for 2 samples) from the size-structure found in the upper layer, with nanoplankton accounting for 69 ± 7% of TC and lower contributions of pico- (18 ± 6%) and microplankton (13 ± 9%).

Although HC (4.0 ± 1.8 g C m^{-2}) and AC (3.5 ± 2.0 g C m^{-2}) were similar on an annual basis (Table 1), there were sampling days (Fig. 3a) and hydrographic phases (Table 1) in which AC was higher than HC. AC exceeded HC during summer upwelling (Phase 2), winter mixing (Phase 6) and spring onset (Phase 7). HC and AC covaried according to an HC:AC ratio = 0.60 ± 0.08 when HC < AC but followed a considerably higher HC:AC ratio = 1.74 ± 0.2 when HC > AC (Fig. 4). HC was particularly high during the summer stratified period (Fig. 3a, Table 1). In fact, when this phase was not included in the relationship between AC and HC, the HC:AC ratio (0.57 ± 0.06; $r^2 = 0.65$; n = 31; $p < 0.001$) was similar to that obtained for samples with AC dominance. During this summer stratified period, HC exceeded AC in both environments, the upper layer (HC:AC = 1.76 ± 0.57) and the SCM (HC:AC = 1.52 ± 056).

Regarding the size structure of the microbial community, heterotrophs clearly dominated year-round in the picoplankton fraction (Fig. 5a), where they accounted for 75 ± 12% of the total picoplankton biomass. The exception was the first sampling during the autumn downwelling of Phase 3 (Fig. 5a), when

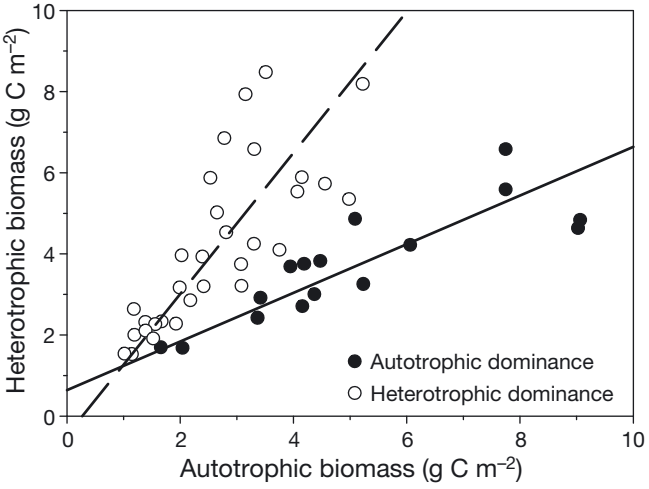

Fig. 4. Heterotrophic to autotrophic plankton biomass relationship for samples with autotrophic dominance (continous line: $y = [0.60 \pm 0.08]x$, $r^2 = 0.72$, n = 16) and samples with heterotrophic dominance (dashed line: $y = [1.74 \pm 0.2]x$, $r^2 = 0.61$, n = 31). Intercepts were not significant for the 2 relationships. See this section of the text for more details

autotrophic picoplankton (APP) slightly exceeded heterotrophic picoplankton (HPP). In contrast, autotrophs and heteretrophs shared importance within nano- (Fig. 5b) and microplankton (Fig. 5c), although autotrophs showed dominance within these 2 fractions during summer upwelling (Phase 2), winter mixing (Phase 6) and the spring onset (Phase 7).

Structure and variability of the autotrophic community

Pico- and nanoplankton cells together with large (>20 µm) diatoms formed the bulk of the autotrophic community, accounting for 98 ± 1% of the AC (Table 2), with autotrophic nanoplankton (ANP) dominating (73 ± 16% of the AC) year-round (Table 2, Fig. 6). Large diatoms and APP (*Synechococcus* and autotrophic picoflagellates) shared similar importance within the autotrophic community (13 ± 18 and 12 ± 8% of AC, respectively), although diatoms showed higher variability (Table 2, Fig. 6a,b). Thus, diatoms were virtually absent from the water column during the autumn downwelling (Phase 3) and the IPC (Phase 5) but co-dominated with ANP during the summer upwelling of Phase 2 (Table 2, Fig. 6b). Such variability was not as evident in APP, although a conspicuous change in composition occurred during the winter upwelling of Phase 4 (Table 2, Fig. 6a). *Synechococcus*, which dominated within this fraction

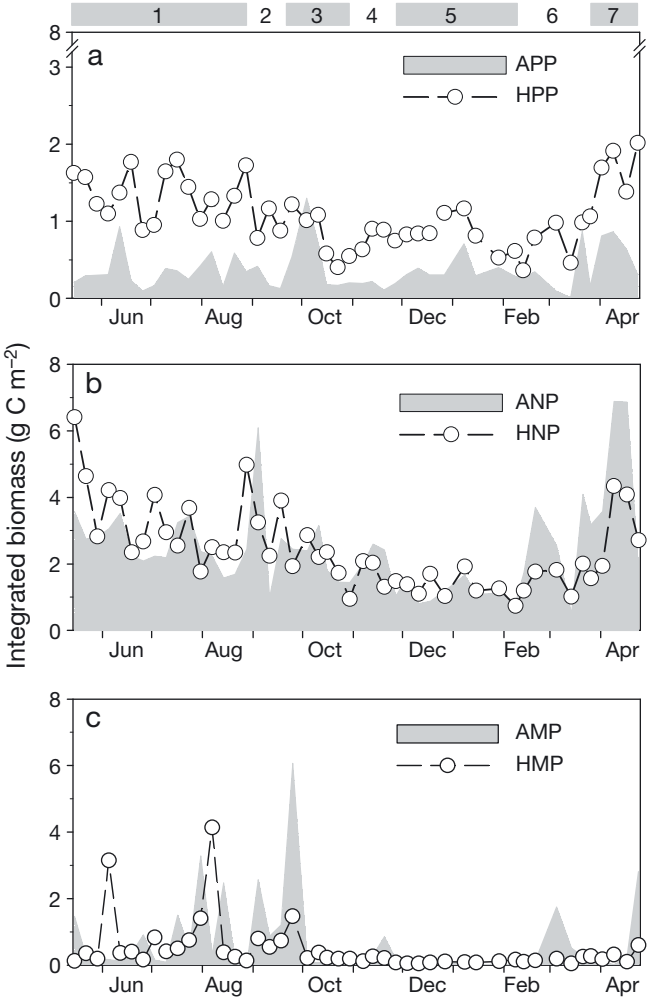

Fig. 5. Evolution of integrated biomass over the photic layer of (a) autotrophic and heterotrophic picoplankton (APP, HPP), (b) autotrophic and heterotrophic nanoplankton (ANP, HNP) and (c) autotrophic and heterotrophic microplankton (AMP, HMP). The 7 hydrographic phases (1 to 7) are given above Panel (a)

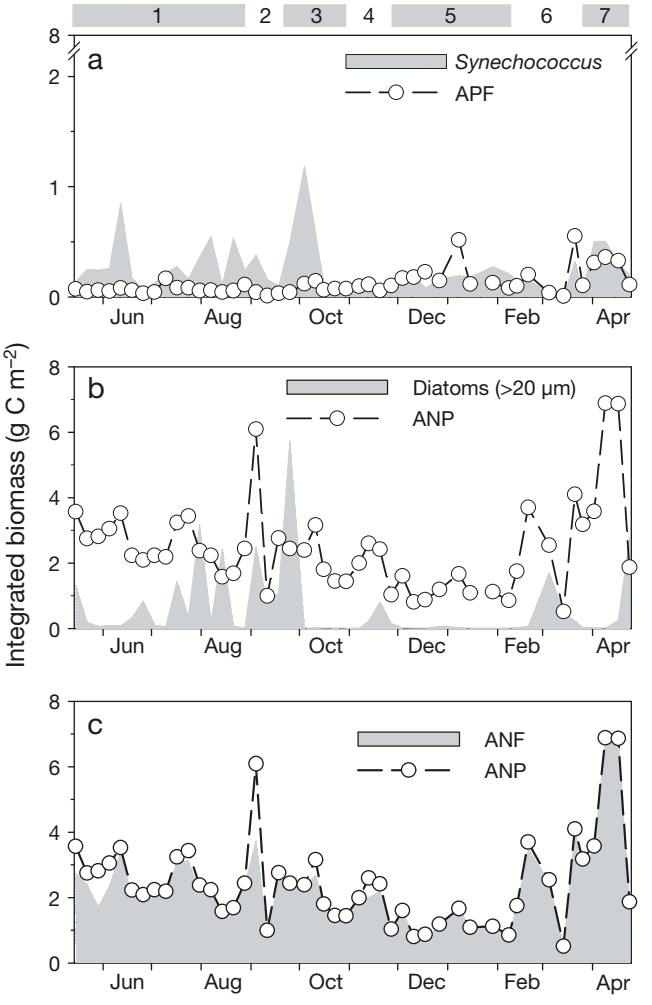

Fig. 6. Evolution of integrated biomass over the photic layer of (a) *Synechococcus* and autotrophic picoflagellates (APF), (b) diatoms larger than 20 µm and total autotrophic nanoplankton (ANP), and (c) autotrophic nanoflagellates (ANF) and ANP. The 7 hydrographic phases (1 to 7) are given above Panel (a)

Table 2. Average (±1 SD) biomass of autotrophic plankton integrated over the photic layer (0.1% of surface irradiance) for the 7 hydrographic phases identified and the whole sampling period. APF: autotrophic picoflagellates; ANP: autotrophic nanoplankton; AD: large (>20 µm) autotrophic dinoflagellates; LAF: large (>20 µm) autotrophic flagellates other than dinoflagellates; ACil: large (>20 µm) autotrophic ciliates; n = number of samples; IPC: Iberian Poleward Current

Hydrographic phase	Biomass (g C m^{-2})						
	Synechococcus	APF	ANP	Diatoms	AD	LAF	ACil
Phase 1 (n = 16) Summer stratification	0.28 ± 0.20	0.07 ± 0.03	2.59 ± 0.63	0.67 ± 0.95	0.07 ± 0.04	0.002 ± 0.01	0.01 ± 0.01
Phase 2 (n = 4) Summer upwelling	0.28 ± 0.19	0.03 ± 0.01	3.07 ± 2.15	2.51 ± 2.28	0.14 ± 0.12	0.003 ± 0.004	0.03 ± 0.04
Phase 3 (n = 5) Autumn downwelling	0.42 ± 0.47	0.09 ± 0.04	2.05 ± 0.73	0.01 ± 0.01	0.03 ± 0.01	0.01 ± 0.01	0.01 ± 0.01
Phase 4 (n = 4) Winter upwelling	0.09 ± 0.18	0.09 ± 0.02	2.01 ± 0.70	0.30 ± 0.36	0.01 ± 0.01	0.02 ± 0.02	0.002 ± 0.002
Phase 5 (n = 8) IPC	0.18 ± 0.06	0.19 ± 0.14	1.15 ± 0.33	0.02 ± 0.02	0.01 ± 0.003	0.005 ± 0.01	0.001 ± 0.001
Phase 6 (n = 5) Winter mixing	0.14 ± 0.12	0.18 ± 0.22	2.52 ± 1.46	0.51 ± 0.70	0.02 ± 0.01	0.02 ± 0.02	0.004 ± 0.002
Phase 7 (n = 5) Spring onset	0.31 ± 0.19	0.24 ± 0.12	4.47 ± 2.28	0.62 ± 1.21	0.03 ± 0.01	0.01 ± 0.01	0.01 ± 0.01
Whole sampling period (n = 47)	0.25 ± 0.22	0.12 ± 0.12	2.47 ± 1.41	0.59 ± 1.11	0.05 ± 0.05	0.01 ± 0.01	0.01 ± 0.02

(78 ± 12% of APP biomass) during summer and autumn (Phases 1 to 3), shared dominance with autotrophic picoflagellates after Phase 4.

Although autotrophic nanoflagellates (ANF) accounted for 92 ± 9% of ANP biomass, other phytoplankton made up important contributions to this autotrophic plankton fraction on some occasions (Fig. 6c). Flagellates like *Heterosigma akashiwo* and *Eutreptiella* sp. accounted for 20 ± 10% of the ANP biomass at the beginning of the summer stratification (Phase 1), and small (<20 µm) diatoms (small centric diatoms and single cells of small *Chaetoceros* spp.) represented 38% of the ANP biomass at the beginning of the summer upwelling (Phase 2). The contribution (19% of the ANP biomass) of small dinoflagellates *Prorocentrum minimum* and *Heterocapsa niei* was also important during the winter upwelling of Phase 4. In contrast, the increase in AC registered at the beginning of the new growth season (Phases 6 and 7, Fig. 3a) was mostly due to ANF, with minor contributions of large diatoms (Table 2, Fig. 6b,c).

The seasonal variability of integrated chl *a* was rather similar to that of AC (Table 1, Fig. 7a). In fact, both variables were significantly correlated ($r = 0.72$, $p < 0.001$), although 3 chl *a* values (2 in winter and 1 in spring) deviated from the general pattern (Fig. 7a). When these 3 pairs of values with low AC to chl *a* ratios of 26 ± 1 (weight:weight) were not considered, the regression between integrated AC and integrated chl *a* (Fig. 7b) provided an AC:chl *a* ratio = 56 ± 5 (slope) with a non-significant intercept (−0.11 ± 0.37). This relationship between chl *a* and AC was basically driven by ANP and diatoms >20 µm, as is illustrated by the regression obtained considering only the autotrophic carbon due to these 2 phytoplankton groups (AC_{anpd}) and total chl *a*: AC_{anpd} = (−0.37 ± 0.34) + (53 ± 5)chl *a* ($r^2 = 0.75$, $p < 0.001$); the intercept was not significant.

During the stratified Phase 1, AC in the SCM represented 67 ± 13% of the water column integrated AC, whereas chl *a* accounted for a higher fraction (76 ± 17%). Consequently, the average AC:chl *a* ratio in the SCM was slightly lower (44 ± 8) than that recorded for the whole sampling (Fig. 7b). However, differences between the size structure and composition of the autotrophic community in the SCM and the water column above were not detected ($0.21 < p < 0.87$, *t*-test for 2 samples). In fact, the size structure in the SCM, with ANP accounting for 78 ± 7% of AC and APP and autotrophic microplankton representing 12 ± 9% and 9 ± 4%, respectively, did not differ from the size structure reported for the whole sampling period ($0.16 < p < 0.89$).

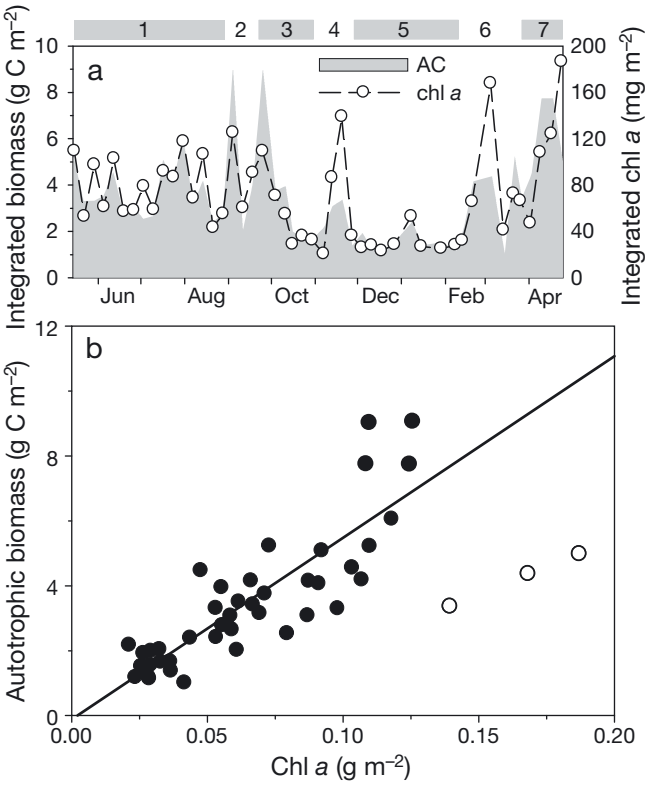

Fig. 7. (a) Evolution of integrated values over the photic layer of total autotrophic plankton biomass (AC) and chlorophyll *a* concentration and (b) relationship between the integrated autotrophic carbon and chlorophyll *a* concentration. In (b), the line corresponds to the equation $y = (-0.11 \pm 0.37) + (56 \pm 5)x$ ($r^2 = 0.74$, $p < 0.001$, $n = 44$) describing the relationship without the 3 open dots. See this section of the text for more details

Structure and variability of the heterotrophic community

The heterotrophic community was dominated by pico- and nanoplankton cells (Table 3), with heterotrophic nanoplankton (HNP) accounting for the largest fraction of HC (61 ± 10%) and heterotrophic bacteria (HB) representing 24 ± 7%. Heterotrophic picoflagellates (HPF) accounted for a smaller fraction (5 ± 3%) of HC. The remaining HC (10 ± 10%) belonged to heterotrophic microplankton (HMP), with large (>20 µm) heterotrophic dinoflagellates (HD) representing 5 ± 5% of HC. Heterotrophic nanoflagellates made up the largest contribution (81 ± 9%) to HNP, with nanodinoflagellates and nanociliates accounting for the remaining HNP biomass.

Seasonal variability was evident in HNP (Fig. 8a) and HD (Fig. 8b), though marked differences existed in the temporal evolution of the biomasses of these 2 heterotrophic plankton groups. HNP gradually de-

Table 3. Average (±1 SD) biomass of heterotrophic plankton integrated over the photic layer (0.1% of surface irradiance) for the 7 hydrographic phases identified and the whole sampling period. HB: heterotrophic bacteria; HPF: heterotrophic picoflagellates; HNP: heterotrophic nanoplankton; HD: large (>20 µm) heterotrophic dinoflagellates; LHF: large (>20 µm) heterotrophic flagellates other than dinoflagellates; HCil large (>20 µm) heterotrophic ciliates; n = number of samples; IPC: Iberian Poleward Current

Hydrographic phase	Biomass (g C m^{-2})					
	HB	HPF	HNP	HD	LHF	HCil
Phase 1 (n = 16) Summer stratification	1.03 ± 0.24	0.33 ± 0.21	3.39 ± 1.24	0.36 ± 0.32	0.38 ± 0.92	0.11 ± 0.07
Phase 2 (n = 4) Summer upwelling	0.89 ± 0.20	0.12 ± 0.05	2.83 ± 0.91	0.59 ± 0.28	0.14 ± 0.12	0.22 ± 0.10
Phase 3 (n = 5) Autumn downwelling	0.62 ± 0.26	0.11 ± 0.05	2.01 ± 0.72	0.14 ± 0.05	0.03 ± 0.01	0.08 ± 0.02
Phase 4 (n = 4) Winter upwelling	0.70 ± 0.16	0.10 ± 0.04	1.72 ± 0.39	0.09 ± 0.03	0.01 ± 0.01	0.07 ± 0.07
Phase 5 (n = 8) IPC	0.67 ± 0.16	0.17 ± 0.18	1.29 ± 0.37	0.05 ± 0.02	0.01 ± 0.003	0.04 ± 0.02
Phase 6 (n = 5) Winter mixing	0.58 ± 0.26	0.13 ± 0.04	1.56 ± 0.43	0.07 ± 0.04	0.02 ± 0.01	0.08 ± 0.06
Phase 7 (n = 5) Spring onset	1.41 ± 0.42	0.20 ± 0.11	2.92 ± 1.25	0.15 ± 0.11	0.03 ± 0.01	0.11 ± 0.17
Whole sampling period (n = 47)	0.88 ± 0.35	0.20 ± 0.16	2.45 ± 1.23	0.23 ± 0.26	0.14 ± 0.55	0.10 ± 0.07

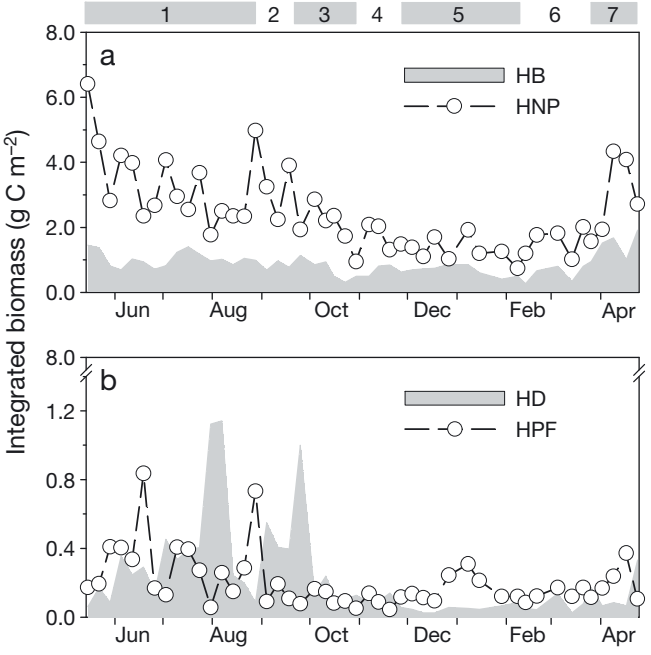

Fig. 8. Evolution of integrated biomass over the photic layer of (a) heterotrophic bacteria (HB) and total heterotrophic nanoplankton (HNP) and (b) heterotrophic dinoflagellates (HD) and heterotrophic picoflagellates (HPF). The 7 hydrographic phases (1 to 7) are given above Panel (a). Note the different scales for Panels (a) and (b)

creased (Fig. 8a, Table 3) from summer stratification (Phase 1) to the IPC (Phase 5). Later on, HNP showed a significant increase ($p < 0.05$, *t*-test for 2 samples) between winter mixing (Phase 6) and the spring onset (Phase 7). In contrast, HD showed a sudden decrease ($p = 0.01$, *t*-test for 2 samples) to low biomass values following the summer upwelling (Phase 2) (Fig. 8b, Table 3). These values remained low until the end of the sampling year. Seasonality was not as evident in HB (Fig. 8a) and HPF (Fig. 8b). Significant changes in HB ($p < 0.01$, *t*-test for 2 samples) were only observed between winter mixing (Phase 6) and the spring onset (Phase 7), when HB increased from 0.58 ± 0.26 to 1.41 ± 0.42 g C m^{-2} (Table 3). Although the biomass of HPF was slightly higher during summer stratification and spring onset (Fig. 8b, Table 3), changes between hydrographic phases were not significant.

There were no differences between the composition of the heterotrophic community found in the SCM and that recorded in the upper layers during Phase 1 ($0.35 < p < 0.98$, *t*-test for 2 samples). Also, the size structure of the heterotrophic community in the SCM was similar to the size structure reported for the whole sampling period ($0.22 < p < 0.78$). HNP dominated in the SCM, accounting for 64 ± 10% of HC, with HPP and HMP representing 26 ± 8 and 11 ± 12%, respectively.

DISCUSSION

The present seasonal study conducted at the NW Iberian shelf clearly shows that both autotrophic and heterotrophic microbial plankton communities in shelf waters of this upwelling system are basically composed of nano- and picoplankton cells. The present study also indicates that microplankton cells are added to or removed from this baseline community according to the prevailing hydrographic regime. Thus, the addition of diatoms >20 µm occurs during summer upwelling events (Fig. 6b), whereas HMP, fundamentally HD, are important components of the microbial community during summer stratified periods (Figs. 5c & 8b). Both autotrophic and heterotrophic microplankton virtually disappear from the water column following the seasonal upwelling-downwelling transition of Phase 3 in autumn (Fig. 5c). In addition, the present study reveals that the spring bloom (Phases 6 and 7) begins with pig-

mented nanoflagellates, with large diatoms making up a minor contribution (Fig. 6). Therefore, we can hypothesise, following Landry (2002) and Barber & Hiscock (2006), that the pelagic food web in this coastal upwelling ecosystem is essentially multivorous (Legendre & Rassoulzadegan 1995). The microbial loop (pico- and nanoplankton) exists as a permanent feature in the system to which the diatom food web is added during upwelling (Barber & Hiscock 2006, Teixeira et al. 2011). During summer upwelling, when diatoms are relatively abundant, their potential HD grazers (Sherr & Sherr 2007, Teixeira et al. 2011) also appear in the water column (Figs. 5c & 8b). The corollary for this structure of the microbial community is that regenerated production and recycling always fuel the pelagic system in the NW Iberian margin, with new production and export being added during upwelling events. In fact, the only study conducted on the NW Iberian shelf addressing microbial metabolism (Teira et al. 2001) supports this view, revealing that the system is net autotrophic only during upwelling events, whereas it is in balance during summer stratification and shifts to heterotrophy under downwelling conditions.

Unfortunately, the metabolic balance of the microbial community was not directly determined during the present study, but it can be estimated using the metabolic theory of ecology (Brown et al. 2004, López-Urrutia et al. 2006), which is based on body size, temperature and resources as main factors determining metabolic rates (López-Urrutia et al. 2006, Cermeño et al. 2008). Thus, following López-Urrutia et al. (2006), phytoplankton metabolic rates (P, mmol O_2 m^{-3} d^{-1}), specifically gross primary production (GPP) and autotrophic respiration (AR) were estimated using their combined model:

$$P = \frac{1}{V} p_0 e^{-E_a/kT} \frac{\mathrm{PAR}}{\mathrm{PAR} + K_m} \sum_{i=1}^{n_a} M_i^{\alpha_a} \qquad (2)$$

where p_0 is a normalization constant that is different for GPP and AR but independent of body size, temperature and light, E_a is the activation energy, k is Boltzmann's constant (8.62×10^{-5} eVK^{-1}), T is the ambient absolute temperature, PAR is the photosynthetic active radiation (mol photons m^{-2} d^{-1}), K_m is the Michaelis-Menten half saturation constant, α_a is the allometric scaling exponent for body size, and n_a is the number of autotrophic organisms in the volume V (m^3) with individual carbon biomass M_i (pg C). E_a, K_m and α_a are the same for GPP and AR (Table 1 in López-Urrutia et al. 2006). PAR was determined at each sampled depth from the incident light at the sea surface and light attenuation profiles recorded on each sampling day (see 'Materials and methods'). Light is the only resource that is explicitly included in the model, whereas nutrients are implicitly considered through cell abundances (n_a) and biomasses M_i, with higher biomass or abundance meaning more available nutrients (Cermeño et al. 2008).

The same equation was used to estimate heterotrophic respiration, except bacterial respiration. For this case, the term PAR/(PAR+K_m) was removed, and the autotrophic parameters E_a and α_a were substituted by those corresponding to heterotrophs (E_h and α_h) (see Table 1 in López-Urrutia et al. 2006).

Bacterial respiration (BR) was estimated from bacterial abundance and the equation given by López-Urrutia & Morán (2007) that relates cell-specific bacterial respiration (BR_i, fg C $cell^{-1}$ d^{-1}) to temperature, taking into account resource availability:

$$BR_i = 3.21 \times 10^{11} e^{-0.589/kT} \qquad (3)$$

Carbon units of BR were converted to oxygen units using a respiration quotient of 0.89.

Keeping in mind that this is a general modelling approach with uncertainties in the outcomes, the net community production (NCP) was calculated by subtracting respiration rates (AR, heterotrophic respiration and BR) from GPP, and then the volumetric values were integrated over the photic layer. The resulting pattern points to an autotrophic microbial community during summer upwelling and spring onset (Table 4). Heterotrophy was mainly located in the picoplankton fraction, where bacteria accounted for 85 ± 7% of total respiration. In contrast, autotrophy was nearly persistent in the microplankton fraction, due to the presence of diatoms. Thus, the 2 hydrographic phases in which microplankton was slightly heterotrophic or almost in balance (autumn downwelling and IPC, respectively) (Table 4) corresponded to phases without diatoms (Table 2). Seasonality was the most evident feature in the metabolic balance of the nanoplankton fraction (Table 4), which showed heterotrophy from autumn downwelling to the end of the IPC (Phases 3 to 5) and autotrophy during the rest of the year. Considering the whole sampling period, the model outcome indicates that the metabolic balance of nano- and microplankton exhibited higher variability than the metabolic balance of picoplankton. This circumstance leads us to conclude that fluctuations in autotrophic biomass, mainly diatoms and nanoflagellates, and the consequent changes in primary production control the transition from net heterotrophy to net autotrophy (Duarte et al. 2001, Arístegui & Harrison 2002, McAndrew et al. 2007, Arbones et al. 2008) in the NW Iberian upwelling.

Table 4. Average (±1 SD) net community production (NCP) of the total microbial community (Total), picoplankton community (Pico), nanoplankton community (Nano) and microplankton community (Micro) integrated over the photic layer (0.1% of surface irradiance) for the 7 hydrographic phases identified and the whole sampling period; n = number of samples. NCP was estimated following the allometric model based on the metabolic theory of ecology proposed by López-Urrutia et al. (2006). IPC: Iberian Poleward Current

Hydrographic phase	NCP (mmol O_2 m^{-2} d^{-1})			
	Total	Pico	Nano	Micro
Phase 1 (n = 16) Summer stratification	−61 ± 115	−92 ± 27	2 ± 73	29 ± 79
Phase 2 (n = 4) Summer upwelling	100 ± 266	−70 ± 21	60 ± 175	110 ± 88
Phase 3 (n = 5) Autumn downwelling	−102 ± 34	−54 ± 14	−42 ± 26	−5 ± 3
Phase 4 (n = 4) Winter upwelling	−65 ± 29	−62 ± 9	−11 ± 20	8 ± 12
Phase 5 (n = 8) IPC	−78 ± 31	−59 ± 19	−17 ± 16	−2 ± 1
Phase 6 (n = 5) Winter mixing	−29 ± 26	−47 ± 21	4 ± 20	15 ± 21
Phase 7 (n = 5) Spring onset	9 ± 83	−101 ± 26	61 ± 44	49 ± 113
Whole sampling period (n = 47)	−44 ± 113	−74 ± 29	4 ± 71	26 ± 68

The level of GPP needed to maintain a balanced metabolism of the microbial community can be obtained by solving the equation describing the relationship GPP vs. NCP (Fig. 9) for NCP = 0. This value of GPP, determining the transition from net heterotrophy to net autotrophy, was 288 mmol O_2 m^{-2} d^{-1} and is equivalent to a mean value of 4.9 mmol O_2 m^{-3} d^{-1} in an average photic layer of 59 ± 14 m. It is also equivalent to a carbon fixation of 3.5 to 2.5 g C m^{-2} d^{-1}, estimated considering a photosynthetic quotient ranging from 1.0 to 1.4. Similar threshold values of GPP have been reported for other coastal upwelling systems (Duarte et al. 2001) and other coastal areas around the world (Duarte et al. 2004, Duarte & Regaudie-de-Gioux 2009) in general, but it is considerably higher than the values reported for the oligotrophic ocean (Arístegui & Harrison 2002, McAndrew et al. 2008, Duarte & Regaudie-de-Gioux 2009).

The threshold of carbon fixation derived from the allometric model is well above the mean annual value of primary production given for the continental shelf of NW Iberia, which lies around 1 to 1.5 g C m^{-2} d^{-1} (Joint et al. 2002, Arístegui et al. 2006). Therefore, it can be concluded that the zone during the present annual study was net heterotrophic. Autotrophy in this region will depend on the frequency and intensity of upwelling events, which could promote an increase in carbon fixation mainly due to diatoms and so fuel the entire metabolism of the microbial community. However, in a possible future scenario with low upwelling intensity and frequency (Álvarez-Salgado et al. 2008), this upwelling zone would become heterotrophic. In this case, the microbial community on the continental shelf should be powered by allochthonous organic inputs, with export from the nearby Rías Baixas, where autotrophy predominates (Arbones et al. 2008), playing a pivotal role.

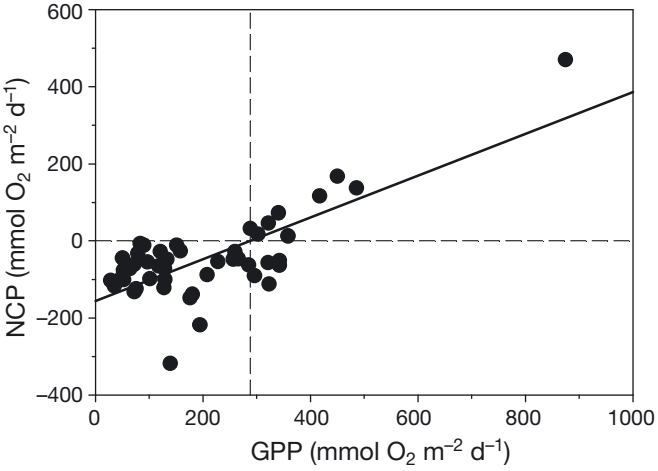

Fig. 9. Net community production (NCP) vs. gross primary production (GPP) estimated according to the allometric model based on the metabolic theory of ecology proposed by López-Urrutia et al. (2006). Continuous line is the regression NCP = (−155.88 ± 18.19) + (0.54 ± 0.07)GPP (r^2 = 0.57, $p < 0.001$, n = 47). The threshold of GPP (vertical dashed line) for net autotrophic production is 288 mmol m^{-2} d^{-1}. The horizontal dashed line shows net metabolic balance (NCP = 0)

Acknowledgements. We thank the captain and crew of the RV 'Mytilus' and the members of the Oceanography group at the Instituto de Investigacións Mariñas who participated in the cruise. This work was funded by the Spanish DYBAGA project (MAR99-1039-C02-01). B.G.C. was supported by a CSIC-ESF I3P fellowship during the experimental work and by a *Juan de la Cierva* contract from the Spanish 'Ministerio de Ciencia e Innovación' during the writing phase. O.E.-G. was supported by a *Mideplan* fellowship from the government of Chile.

LITERATURE CITED

Álvarez-Salgado XA, Figueiras FG, Pérez FF, Groom S and others (2003) The Portugal coastal counter current off NW Spain: new insights on its biogeochemical variability. Prog Oceanogr 56:281–321

Álvarez-Salgado XA, Labarta U, Fernández-Reiriz MJ, Figueiras FG and others (2008) Renewal time and the impact of harmful algal blooms on the extensive mussel raft culture of the Iberian coastal upwelling system (SW Europe). Harmful Algae 7:849–855

Arbones B, Castro CG, Alonso-Pérez F, Figueiras FG (2008) Phytoplankton size structure and water column metabolic balance in a coastal upwelling system: the Ría de Vigo, NW Iberia. Aquat Microb Ecol 50:169–179

Arístegui J, Harrison WG (2002) Decoupling of primary production and community respiration in the ocean: implications for regional carbon studies. Aquat Microb Ecol 29: 199–209

Arístegui J, Álvarez-Salgado XA, Barton ED, Figueiras FG, Hernández-León S, Roy C, Santos AMP (2006). Oceanography and fisheries of the Canary Current/Iberian region of the Eastern North Atlantic. In: Robinson AR, Brink KH (eds) The sea, Vol 14: the global coastal ocean: interdisciplinary regional studies and synthesis. Harvard University Press, Cambridge, MA, p 879–933

Azam F, Fenchel T, Field JG, Gray JS, Meyer-Reil LA, Thingstad F (1983) The ecological role of water-column microbes in the sea. Mar Ecol Prog Ser 10:257–263

Bakun A (1973) Coastal upwelling indices, west coast of North America 1946-71. NOAA Tech Rep, NMFS SSRF-671, US Dept of Commerce, Seattle, WA

Barber RT, Hiscock MR (2006) A rising tide lifts all phytoplankton: growth response of other phytoplankton taxa in diatom-dominated blooms. Global Biogeochem Cycles 20, GB4S03, doi:10.1029/2006GB002726

Böttjer D, Morales CE (2007) Nanoplanktonic assemblages in the upwelling area off Concepción (~36° S), central Chile: abundance, biomass, and grazing potential during the annual cycle. Prog Oceanogr 75:415–434

Bratbak G, Dundas I (1984) Bacterial dry matter content and biomass estimation. Appl Environ Microbiol 48:755–757

Brown JM, Gillooly JF, Allen AP, Savage VM, West GB (2004) Toward a metabolic theory of ecology. Ecology 85: 1771–1789

Castro CG, Álvarez-Salgado XA, Figueiras FG, Pérez FF, Fraga F (1997) Transient hydrographic and chemical conditions affecting microplankton populations in the coastal transition zone of the Iberian upwelling system (NW Spain) in September 1986. J Mar Res 55:321–352

Cermeño P, Marañón E, Harbour D, Figueiras FG and others (2008) Resources levels, allometric scaling of population abundance, and marine phytoplankton diversity. Limnol Oceanogr 53:312–318

Crespo BG, Figueiras FG (2007) A spring poleward current and its influence on microplankton assemblages and harmful dinoflagellates on the western Iberian coast. Harmful Algae 6:686–699

Crespo BG, Figueiras FG, Groom S (2007) Role of across-shelf currents in the dynamics of harmful dinoflagellate blooms in the northwestern Iberian upwelling. Limnol Oceanogr 52:2668–2678

Cushing DH (1989) A difference in structure between ecosystems in strongly stratified waters and in those that are only weakly stratified. J Plankton Res 11:1–13

Duarte CM, Regaudie-de-Gioux A (2009) Thresholds of gross primary production for the metabolic balance of marine planktonic communities. Limnol Oceanogr 54:1015–1022

Duarte CM, Agustí S, Arístegui J, González N, Anadón R (2001) Evidence for a heterotrophic subtropical northeast Atlantic. Limnol Oceanogr 46:425–428

Duarte CM, Agustí S, Vaqué D (2004) Controls on planktonic metabolism in the Bay of Blanes, northwestern Mediterranean littoral. Limnol Oceanogr 49:2162–2170

Fermín EG, Figueiras FG, Arbones B, Villarino ML (1996) Short-time scale development of a *Gymnodinium catenatum* population in the Ría de Vigo (NW Spain). J Phycol 32:212–221

Figueiras FG, Labarta U, Fernández-Reíriz MJ (2002) Coastal upwelling, primary production and mussel growth in the Rías Baixas of Galicia. Hydrobiologia 484: 121–131

Frouin R, Fiúza AFG, Ambar I, Boyd TJ (1990) Observations of a poleward surface current off the coasts of Portugal and Spain during winter. J Geophys Res 95:679–691

Goldman JC (1988) Spatial and temporal discontinuities of biological processes in pelagic surface waters. In: Rothschild BJ (ed) Toward a theory on biological-physical interactions in the world ocean. Kluwer Academic, Dordrecht, p 273–296

Hansen HP, Grasshoff K (1983) Automated chemical analysis. In: Grasshoff K, Ehrhardt M, Kremling K (eds) Methods of seawater analysis. Verlag Chemie, Weinheim, p 347–379

Hillebrand H, Dürselen C, Kirschtel D, Pollingher U, Zohary T (1999) Biovolume calculation for pelagic and benthic microalgae. J Phycol 35:403–424

Iriarte JL, González HE (2004) Phytoplankton size structure during and after the 1997/98 El Niño in a coastal upwelling area of the northern Humboldt Current System. Mar Ecol Prog Ser 269:83–90

Joint I, Groom SB, Wollast R, Chou L and others (2002) The response of phytoplankton production to periodic upwelling and relaxation events at the Iberian shelf break: estimates by the ^{14}C method and by satellite remote sensing. J Mar Syst 32:219–238

Landry MR (2002) Integrating classical and microbial food web concepts: evolving views from the open-ocean tropical Pacific. Hydrobiologia 480:29–39

Legendre L, Rassoulzadegan F (1995) Plankton and nutrient dynamics in marine waters. Ophelia 41:153–172

Lessard EJ, Swift E (1986) Dinoflagellates from the North Atlantic classified as phototrophic or heterotrophic by epifluorescence microscopy. J Plankton Res 8:1209–1215

Linacre LP, Landry MR, Lara-Lara JR, Hernandez-Ayon JM, Bazan-Guzman C (2010) Picoplankton dynamics during contrasting seasonal oceanographic conditions at a coastal upwelling station off Northern Baja California, Mexico. J Plankton Res 32:539–557

López-Urrutia A, Morán XAG (2007) Resource limitation of bacterial production distorts the temperature dependence of oceanic carbon cycling. Ecology 88:817–822

López-Urrutia A, San Martin E, Harris RP, Irigoien X (2006) Scaling the metabolic balance of the oceans. Proc Natl Acad Sci USA 103:8739–8744

Lorenzo LM, Arbones B, Tilstone GH, Figueiras FG (2005) Across-shelf variability of phytoplankton composition, photosynthetic parameters and primary production in the NW Iberian upwelling system. J Mar Syst 54:157–173

Margalef R (1978) Life forms of phytoplankton as survival alternatives in an unstable environment. Oceanol Acta 1: 493–509

McAndrew PM, Björkman KM, Church MJ, Morris PJ, Jachowski N, Williams PJ le B, Karl DK (2007) Metabolic response of oligotrophic plankton communities to deep water nutrient enrichment. Mar Ecol Prog Ser 332:63–75

McAndrew PM, Bidigare RR, Karl DM (2008) Primary production and implications for metabolic balance in Hawaiian lee eddies. Deep-Sea Res II 332:63–75

Morán XAG, Gasol JM, Pedrós-Alió C, Estrada M (2002) Partitioning of phytoplanktonic organic carbon production and bacterial production along a coastal-offshore gradient in the NE Atlantic during different hydrographic regimes. Aquat Microb Ecol 29:239–252

Peliz A, Dubert J, Santos AMP, Oliveira PB, Le Cann B (2005) Winter upper ocean circulation in the Western Iberia Basin — fronts, eddies and poleward flows: an overview. Deep-Sea Res I 52:621–646

Pomeroy LR (1974) The ocean's food web, a changing paradigm. Bioscience 24:499–504

Porter KG, Feig YS (1980) The use of DAPI for identifying and counting aquatic microflora. Limnol Oceanogr 25: 943–948

Putt M, Stoecker DK (1989) An experimentally determined carbon:volume ratio for marine 'oligotrichous' ciliates from estuarine and coastal waters. Limnol Oceanogr 34: 1097–1103

Rodríguez F, Garrido JL, Crespo BG, Arbones B, Figueiras FG (2006) Size-fractionated phytoplankton pigment groups in the NW Iberian upwelling system: impact of the Iberian Poleward Current. Mar Ecol Prog Ser 323: 59–73

Ryther JH (1969) Photosynthesis and fish production in the sea. Science 166:72–76

Sherr EB, Sherr BF (2007) Heterotrophic dinoflagellates: a significant component of microzooplankton biomass and major grazers of diatoms in the sea. Mar Ecol Prog Ser 352:187–197

Sherr EB, Sherr BF, Wheeler PA (2005) Distribution of coccoid cyanobacteria and small eukaryotic phytoplankton in the upwelling ecosystem off the Oregon coast during 2001 and 2002. Deep-Sea Res II 52: 317–330

Strathmann R (1967) Estimating the organic carbon content of phytoplankton from cell volume or plasma volume. Limnol Oceanogr 12:411–418

Teira E, Serret P, Fernández E (2001) Phytoplankton size-structure, particulate and dissolved organic carbon production and oxygen fluxes through microbial communities in the NW Iberian coastal transition zone. Mar Ecol Prog Ser 219:65–83

Teixeira IG, Figueiras FG, Crespo BG, Piedracoba S (2011) Microzooplankton feeding impact in a coastal upwelling system on the NW Iberian margin: the Ría de Vigo. Estuar Coast Shelf Sci 91:110–120

Tilstone GH, Figueiras FG, Lorenzo LM, Arbones B (2003) Phytoplankton composition, photosynthesis and primary production during different hydrographic conditions at the Northwest Iberian upwelling system. Mar Ecol Prog Ser 252:89–104

Torres R, Barton ED (2006) Onset and development of the Iberian poleward flow along the Galician coast. Cont Shelf Res 26:1134–1153

Varela M, Díaz del Río G, Álvarez-Ossorio MT, Costas E (1991) Factors controlling phytoplankton size class distribution in the upwelling area of the Galician continental shelf (NW Spain). Sci Mar 55:505–518

Vargas CA, Martínez RA, Cuevas LA, Pavez MA and others (2007) The relative importance of microbial and classical food webs in a highly productive coastal upwelling area. Limnol Oceanogr 52:1495–1510

Verity PG, Langdon C (1984) Relationships between lorica volume, carbon, nitrogen and ATP content of tintinnids in Narraganssett Bay. J Plankton Res 6:859–868

Verity PG, Robertson CY, Tronzo CR, Andrews MG, Nelson JR, Sieracki ME (1992) Relationships between cell volume and the carbon and nitrogen content of marine photosynthetic nanoplankton. Limnol Oceanogr 37: 1434–1446

Wooster WS, Bakun A, McLain DR (1976) The seasonal upwelling cycle along the eastern boundary of the North Atlantic. J Mar Res 34:131–141

Editorial responsibility: Hans-Georg Hoppe, Kiel, Germany

Submitted: December 13, 2011; Accepted: July 11, 2012
Proofs received from author(s): September 6, 2012